Jurnal Teknologi

Full Paper

RADIATION CHARACTERISTIC OF CLOUD BASED MAGNETOMETER FOR VEHICLE DETECTION

S. K. Yee[a], M. C. Teoh[f], Z. Z. Abidin[b], S. H. Dahlan[a], M. R. Annual[a], K. S. Tee[d], D. Lim[e], C. H. See[c], H. Zhang[c], Y. Zheng[g], C. F. Soon[f*]

[a]Research Center for Applied Electromagnetic, Universiti Tun Hussein Onn Malaysia, 86400 Parit Raja, Johor, Malaysia
[b]Advanced Wireless Communication Research Centre (ATRC), Faculty of Electrical and Electronic Engineering, Universiti Tun Hussein Onn Malaysia, 86400 Parit Raja, Johor, Malaysia
[c]School of Engineering & the Built Environment, Edinburgh Napier University, United Kingdom
[d]Faculty of Electrical and Electronic Engineering, Universiti Tun Hussein Onn Malaysia, 86400 Parit Raja, Johor, Malaysia
[e]SENA traffic system Sdn. Bhd., 30, Jln Radin Bagus 3, Bandar Baru Sri Petaling, 57000 Kuala Lumpur, Malaysia
[f]Microelectronics and Nanotechnology-Shamsuddin Research Centre, Universiti Tun Hussein Onn Malaysia, 86400 Parit Raja, Johor, Malaysia
[g]School of Environment and Civil Engineering, Dongguan University of Technology, China

Article history
Received
29 August 2022
Received in revised form
11 December 2022
Accepted
26 December 2022
Published Online
23 February 2023

*Corresponding author
soon@uthm.edu.my

Graphical abstract

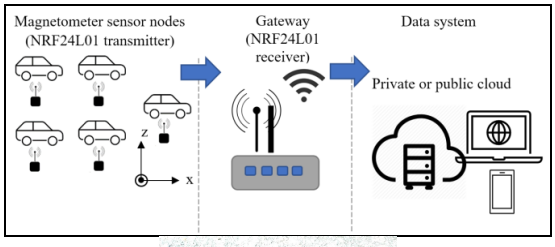

Abstract

A traffic sensing and monitoring system based on a magnetometer is proposed to work with Arduino pro-mini and nRF24L01 to mitigate traffic congestion problems. As vehicles pass through the magnetometer buried underground, the microcontroller processes the magnetic field changes and transmits them by the nRF24L01 transceiver for data analysis. A MIFA antenna resonating at 2.4 GHz is incorporated in the transceiver module for transmission purposes. The performance of this antenna is simulated by using COMSOL commercial software. Approximate 7 dB of return loss enhancement is found when taper design is applied to the antenna. Since the antenna is designed to radiate at 2.4 GHz, its antenna gain is the highest (1.22 dBi) in this frequency too. The simulated 3D and 2D gain patterns have shown that this antenna is radiating omnidirectional, suitable for transmitting signals in all directions. This is further validated by the Received Signal Strength Indicator (RSSI) measurement, which indicates a similar trend of signal strength for all locations at a distance below 40 m (-87 dBm). When the distances increase beyond 40 m, the RSSI at the direction closer to the traffic flow drops significantly compared to the other directions where 30 dBm of variation is detected at 100 m.

Keywords: Traffic sensing, magnetometer, nRF24L01, MIFA antenna, Received Signal Strength Indicator (RSSI)

Abstrak

Sistem penderiaan dan pemantauan lalu lintas berdasarkan magnetometer dicadangkan untuk berfungsi dengan Arduino pro-mini dan nRF24L01 untuk mengurangkan masalah kesesakan lalu lintas. Apabila kenderaan melalui magnetometer yang ditanam di bawah tanah, mikropengawal memproses perubahan medan magnet dan menghantarnya oleh transceiver nRF24L01 untuk analisis data. Antena MIFA yang bergema pada 2.4 GHz digabungkan dalam modul transceiver untuk tujuan penghantaran. Prestasi antena ini disimulasikan dengan menggunakan perisian komersial COMSOL. Didapati bahawa reka bentuk tirus meningkatkan kehilangan pulangan antenna sebanyak 7 dB. Memandangkan antena direka untuk memancar pada 2.4 GHz, perolehan antenanya adalah yang tertinggi (1.22 dBi) dalam frekuensi ini juga. Corak keuntungan 3D dan 2D yang disimulasikan telah menunjukkan bahawa antena ini memancarkan omnidirectional, sesuai untuk menghantar isyarat ke semua arah. Ini selanjutnya disahkan oleh ukuran Penunjuk Kekuatan Isyarat Diterima (RSSI), yang menunjukkan arah aliran kekuatan isyarat yang serupa pada jarak di bawah 40 m. Apabila jarak meningkat melebihi 40 m, RSSI pada arah yang lebih dekat dengan aliran trafik menurun dengan ketara berbanding dengan arah lain dimana sebanyak 30 dBm perbezaan pada jarak 100 m.

Kata kunci: Penderiaan lalu lintas, magnetometer, nRF24L01, MIFA antena, Penunjuk Kekuatan Isyarat yang Diterima (RSSI)

1.0 INTRODUCTION

Traffic management control is applied to improve the traffic congestion and efficiency especially in urban area. It includes sensing, traffic data monitoring/analysis, regulation, control and telecommunication for all the transportations on the road [1]. Most traffic problems originate from unavailable information such as timing, accurate traffic information and coordination between the system. Information and communication technologies could enable an intelligent transport system. Inductive loop detectors, ultrasonic, radar, video image detectors (VID), visual images from closed-circuit television (CCTV) and magnetic sensor are commonly used to monitor complicated traffic information. The information collected at the traffic management centre will be processed, verified and organized using the data fusion process for analysis [2]. The traffic information can be disseminated in various communications systems to the travellers to improve transportation efficiency and safety. In a more complex information system, the traffic information is linked to the traffic controller center and coordinating the traffic lights in the adjacent junctions and intelligently control the flow of vehicles, leading to mitigating traffic congestion problems [3].

2.0 WIRELESS HARDWARE SYSTEM AND CLOUD PLATFORM

The wireless magnetometer consists of a HMC5883L magnetic sensor (Honeywell) [4], Arduino pro-mini [5], and nRF24L01 transceiver module from Nordic Semiconductor [6]. The three modules were designed on a single board, as shown in Figure 1. HMC5883L is a triaxial anisotropic Magnetoresistive sensor with a 12-bit analog-to-digital converter and 1 to 2° compass heading accuracy [7]. Any distortion on the magnetic sensor would generate a change of data for the x-, y- and z-axis. The data output was acquired via I^2C serial bus to the microcontroller. The nRF24L01 transceiver module is based on the Industrial, Scientific, and Medical (ISM) frequency band and utilizes Gaussian Frequency Shift Keying (GFSK) modulation. The output power (0 dBm), and data rate (250kbps) are configurable through SPI interface. However, lower data rate yields with higher receiver sensitivity. nRF24L01 is a suitable communication technology for designing standalone devices because the current consumed is 12 mA during transmission at 0dBm and 26 µA in standby mode. nRF24L01 has an onboard antenna that supports an open-air transmission range of 100 meter. The transmission distance is extendable to 1000 m using a receiver with a Power Amplifier (PA) and Low Noise Amplifier (LNA) module. This increased the detection of extremely weak signals from the antenna down to -100 dBm.

The data packet received at the receiver or gateway will be decoded and the microcontroller will direct information at the gateway to an ESP8266-01 Wi-Fi module [8]. The module connects to a designated network SSID with a password under IEEE 802.11 standard. Subsequently, the Wi-Fi module posted the data and device identification via the Application Protocol Interface (API) protocol to

Ubidot Cloud. A specific token provided by Ubidot identified the authentication. The data transfer will be displayed on a dashboard developed in this research. It has specific URL to be accessed via mobile phone and computer desktop. The traffic data with time stamps could be continuously stored in the cloud storage server. Besides the information mentioned above, the sensing system is able to display the receive signal strength and the time where the vehicles are detected. The explained magnetometer sensing system is illustrated in Figure 2.

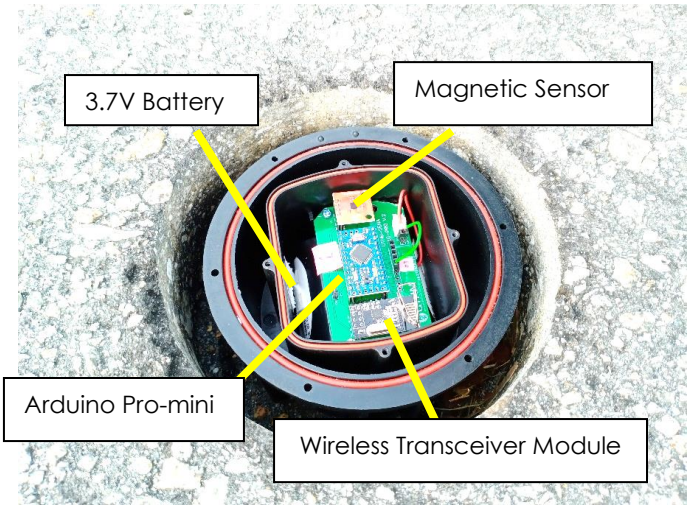

Figure 1 The developed magnetometer sensor is buried 15 cm underground

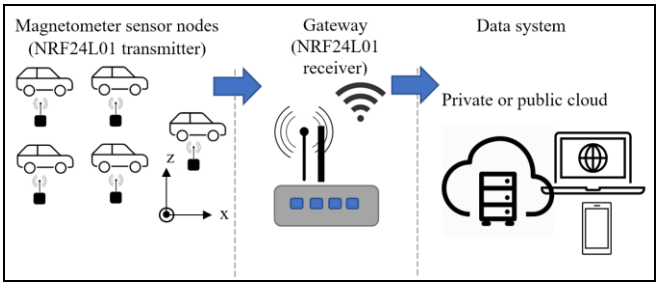

Figure 2 Overall cloud-based magnetometer system diagram

2.1 Investigation of the Receive Signal Strength Indicator (RSSI) and Transmission Power Reception of nRF24L01 for Point-to-point Communication

The signal strength level of the module was measured at four (4) different locations: A, B, C and D, as shown in Figure 3. The module is located at the arranged distance, *d* from 10 m up to 100 m, from the receiver. A 20 cm diameter wide and 15 cm depth of hole is made to bury the magnetometer sensor. After allocating the module and receiver, the signal strength values are collected. In actual application, the sensing systems will be installed at each traffic light junctions. Since these sensors are far apart from each other and buried underground, they will not interfere with each other.

Receive Signal Strength Indicator (RSSI), expressed in dBm, represents the relationship between a transmitted and received power. It was used to calculate the distance between a transmitter and a receiver when the most signal propagates in a Line-of-Sight (LOS). Higher RSSI values indicate a stronger signal. The measured and estimated RSSI values are later will be compared with the theoretical RSSI value based on the Free-Space Path Loss (FSPL) model equation (1) given by [9], where *K* is a constant represented by (2), *d* is the distance between the transmitter and the receiver, *f* is the frequency of the RF signal, *c* is the speed of light and *Pt* denotes the transmitted power.

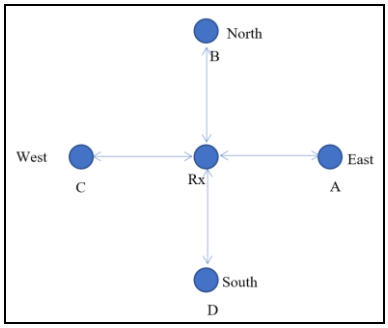

Figure 3 Experimental setup positions of location A, B, C and D

$$RSSI = -20 \log_{10} (d) + K \quad (1)$$

where

$$K = 10 \log_{10} (P_t) - 20 \log_{10} (4\pi f) + 20 \log_{10} (c) \quad (2)$$

2.2 Modeling the Radiation Characteristic of MIFA Antenna of NRF14L01

The whole simulation process is done mainly in COMSOL Multiphysics version 5.6 [10], [11].

Model wizard followed by 3D is selected at the startup window. This software has various modules to cater for objects that operate under different fields of physics, ranging from AC/DC to Structural Mechanics. The most suitable module for MIFA (antenna) simulation is the Radio Frequency (RF) Module, since the transceiver runs at 2.4 GHz. This module analyses the electric and magnetic fields in systems of high frequencies, which corresponds to devices whose sizes are comparable to the operating wavelength. Within the RF module, the "Electromagnetic Waves, Frequency Domain (emw)" physics interface is chosen, and then the "frequency domain" study is added.

The description and parameters of the design are shown in Table 1 and Figure 4, respectively. Figure 5 shows the MIFA antenna model with lumped port and vias constructed in the software.

The designed model does not consider the effect of soil, enclosure and other electronic components on the boards as that causes long computation time.

Upon completing the 3D geometry, assigning materials and physics involved in the model is completed based on the material library in the software. The copper is selected for the antenna, transmission lines, vias and ground planes, while FR4 is selected for the substrate (Circuit board). A perfectly matched layer (PML) is selected in this design. It is an imaginary layer that absorbs all incoming waves and thus leaves no reflection that might cause a disturbance in the calculations. Lumped ports are defined as an excitation source for the model and the voltage is set at 5 Volts. A total of 200 data point of S11 is simulated from 2 GHz to 3 GHz.

Table 1 List of parameters to be used in the simulation. Refer to Figure 4 for parameters description

Symbol	Value	Description
Lg	593 mils	Length of PCB
Wg	1280 mils + 0.5 mm	Width of PCB
L	435 mils	Length of MIFA
W	280 mils	Width of MIFA
f	2.4GHz	Frequency
lambda	c_const/f	Wavelength
PMLt	0.1*lambda/4	PML thickness
PMLr	lambda/4	PML radius
tW	65 mils	-
S	12 mils	Gaps neigbouring tW
t0	65 mils	-
t1	25 mils	-
t2	20 mils	-
t3	273 mils	-
ta	0.035 mm	MIFA thickness
tp	1.6 mm	PCB thickness
tr	7.5 mm	Via radius
vs	379/9 mils	Via spacing

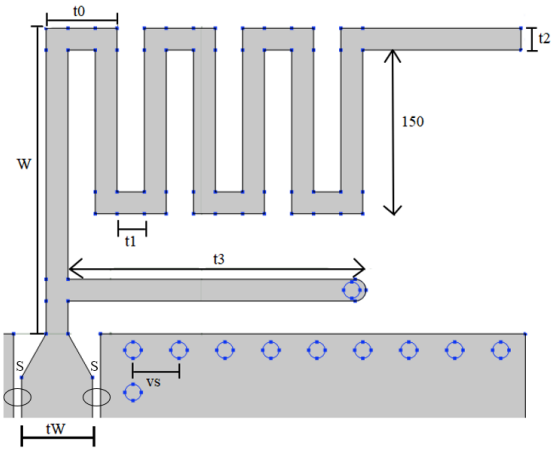

Figure 4 Parameters of the antenna structure. "S" represents the gaps neighbouring "tW"

3.0 RESULTS AND DISCUSSION

3.1 Parametric Study on The Effect Taper Length of MIFA Antenna

A taper is introduced to connect the enlarged feeding copper trace (65 mils) and the MIFA antenna (20 mils) for impedance matching, as shown in Figure 6. It is important to ensure that the 50 Ohm feedline matches the impedance of the antenna because almost all microwave instruments are manufactured with this impedance. Mismatching creates unwanted reflection, standing waves and hence less power transmitted to the system or across the free space for antenna application. Proper impedance matching can optimize antenna performance such as return loss, bandwidth, and resonance frequency [12]. It can be proven from the simulation results (S11) of different taper lengths, 0 mils (L0), 40 mils (L40), 60 mils(L60) and 80 mils(L80), as shown in Figure 7. The amplitude of the return loss, resonance frequency and bandwidth of the MIFA antenna are tabulated in Table 2.

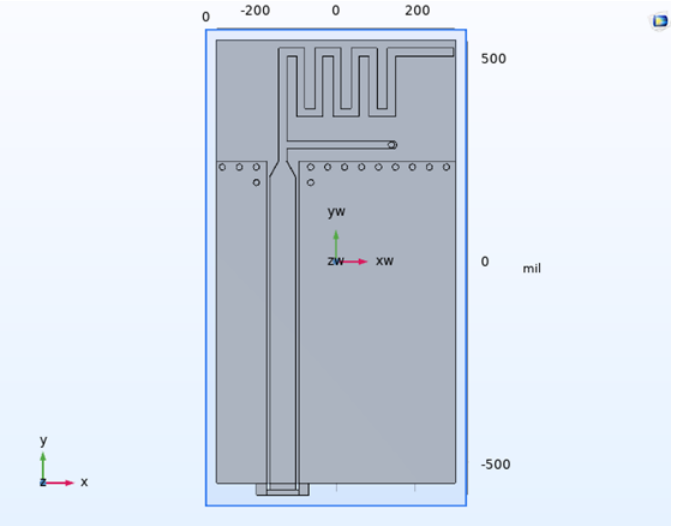

Figure 5 The top view of the MIFA antenna with lumped port and vias

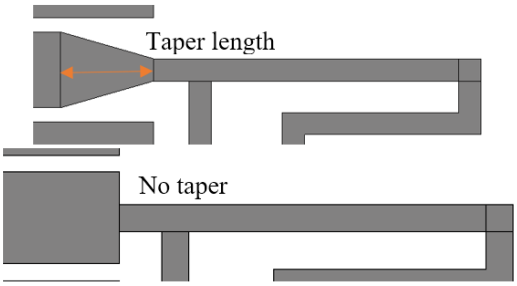

Figure 6 The effect of taper length is investigated

It is observed that the introduction of the taper has enhanced the return loss of the MIFA antenna and this improvement is inversely proportional to taper length. The taper allows the gradual impedance variation (changes of width) [13], unlike when no taper is defined in the design. The highest return loss (S11) of -27.51 dB is reported when the taper length is 20 mils, while the lowest happens when there is no taper (-20.23 dB), the return loss is tabulated in Table 2. Interestingly, keeping a long taper length does not promise a better return loss. At the same time, it is also found that varying the taper length has a mild effect on the resonance frequency shifting of the antenna [14]. MIFA antenna is widely used as the radiating antenna in module because it radiates in omi-directional. It has shorter radiating element hence make it more compact for system miniaturization [15]. The highest bandwidth of 215.37 MHz is obtained when the taper length is 20 mils. It is followed by 214.03 MHz, 208.67 MHz and 199.29 MHz for taper lengths of 40 mils, 60 mils and 80 mils, respectively. The lowest bandwidth, 181.16 MHz is found when there is no taper. Based on this parametric study, a taper length of 20 mils has been selected as it offers the widest bandwidth and highest return loss.

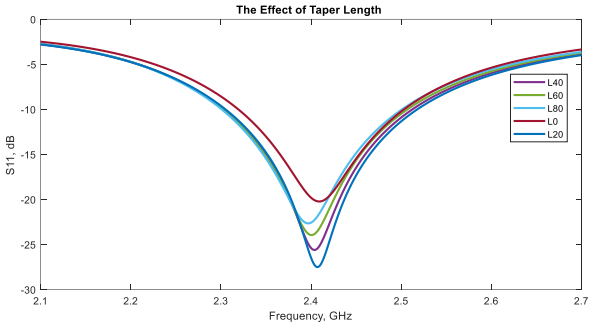

Figure 7 The return loss of the antenna when the taper length is varied

Table 2 The return loss, resonance frequency and bandwidth of MIFA antenna with different taper length

Taper length, mils	Resonance frequency, GHz	Bandwidth, MHz	Return loss, dB
0 (L0)	2.409	181.16	-20.23
20 (L20)	2.407	215.37	-27.51
40 (L40)	2.404	214.03	-25.60
60 (L60)	2.401	208.67	-23.96
80 (L80)	2.397	199.29	-22.66

3.2 3D and 2D Far-Field Gain Radiation Pattern

The 3D far-field gain radiation pattern of the antenna for 2 GHz, 2.2513 GHz, 2.402 GHZ, 2.7337 GHz, 3 GHz computed from the simulation are shown in Figure 8 (a) to (e). All the radiation patterns are presented in torus shape. They are omi-directional, expected for a quarter-wave monopole antenna like the MIFA [15]. At a frequency 2 GHz and 3 GHz, the antenna's gain is a negative value, which indicates it does not radiate; instead, it dissipates the energy. While at 2.513 GHz, 2.4 GHz and 2.7337 GHz, the antenna has positive gain to radiate the signal. The highest gain is achieved at 2.4 GHz, which is the resonance frequency of the MIFA antenna as stated in the simulation and data sheet. The shape of the torus deformed as the frequency moved to 3 GHz.

The radiation direction of the antennas can be illustrated clearly by referring to the 2D gain radiation pattern in Figure 9. The 2D far-field gain pattern plots the MIFA's radiation pattern by referring to one of the selected planes (usually either XY, XZ or YZ plane). In this simulation, the plane at θ=90° (XY plane) is chosen. There are two main lobes focused in the 0° and 180° directions.

3.3 Resonance Frequency and Bandwidth of MIFA Antenna

Figure 10 shows the return loss (S11) of the antenna from 2 GHz to 3 GHz. Based on the figure, the resonance frequency of the antenna is 2.407 GHz. At this frequency, the return loss magnitude is -27.18 dB, which means the antenna reflects approximate 19% of the energy and the remaining 81% of energy is successfully radiated by the MIFA antenna [16]. This percentage can be calculated by (3).

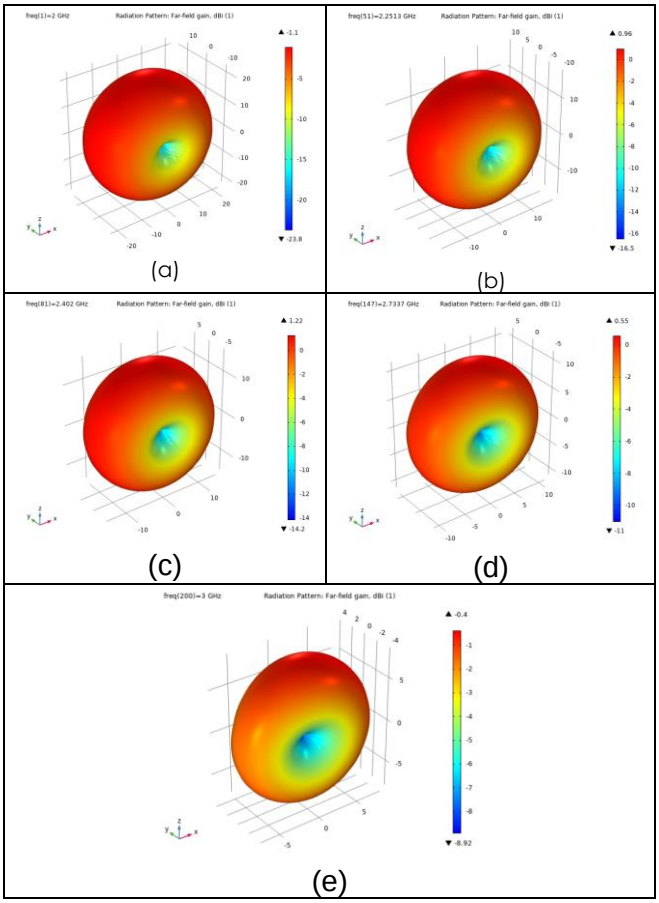

Figure 8 3D far-field gain pattern for (a) 2 GHz, (b) 2.2513 GHz, (c) 2.402 GHZ, (d) 2.7337 GHz, (e) 3 GHz

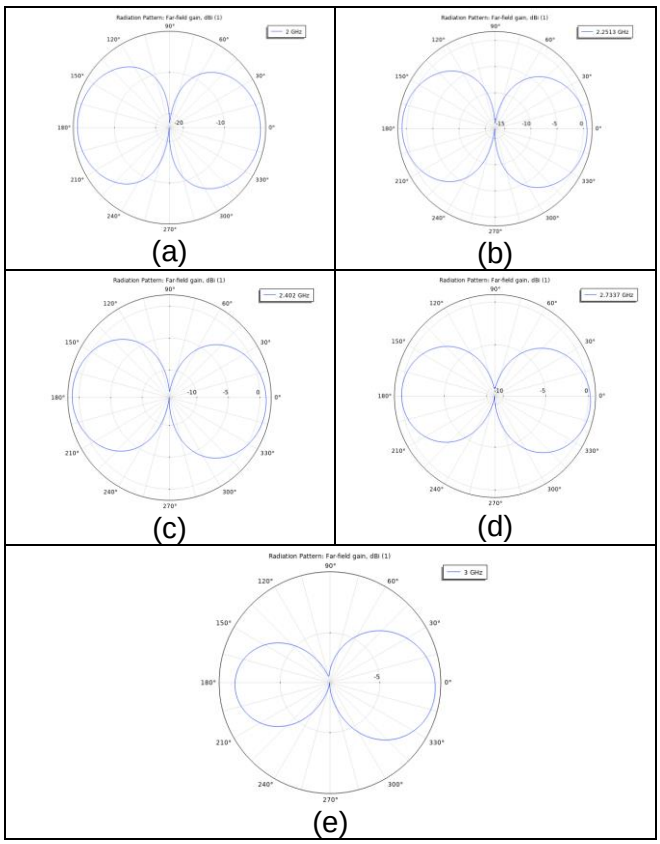

Figure 9 2D far-field gain pattern for (a) 2 GHz, (b) 2.2513 GHz, (c) 2.402 GHZ, (d) 2.7337 GHz, (e) 3 GHz

$$S_{11} = 10 \log \frac{\text{Reflected Energy}}{\text{Incident Energy}} \quad (3)$$

The bandwidth of this antenna can be measured by finding the difference between the upper frequency and lower frequency at -10 dB, as shown in Figure 10. According to the calculation, the bandwidth of the antenna is 215.37 MHz.

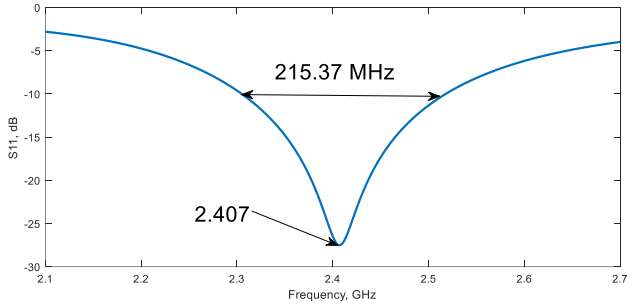

Figure 10 Return loss (S11) of MIFA antenna

3.4 RSSI and Transmission Power Reception of NRF24L01 at Different Angles and Distances for Point-To-Point Communication

The performance of the proposed system in performing transmission and reception within a specific range has been conducted in a real environment. The practical experiments were conducted in an open area, Padang Kawad, Universiti Tun Hussein Onn Malaysia, to observe the Received Signal Strength Indicator (RSSI) level in function of the distance. The NRF24L01 module and Rohde and Schwarz FSH8 handheld spectrum analyzer [17] are used as the transmitter and the receiver, respectively. The experimental setup for data collection is depicted in Figure 11. Dipole antenna is used to capture the signal from the NRF2410 transceiver. The height of receiving antenna is 1.8 m, as shown in Figure 12.

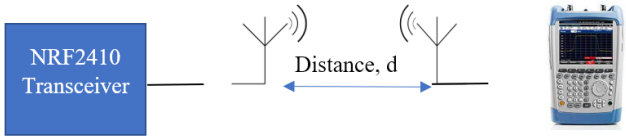

Figure 11 Illustration of the experimental setup

Figure 12 Dipole antenna is used as receiver in the measurement

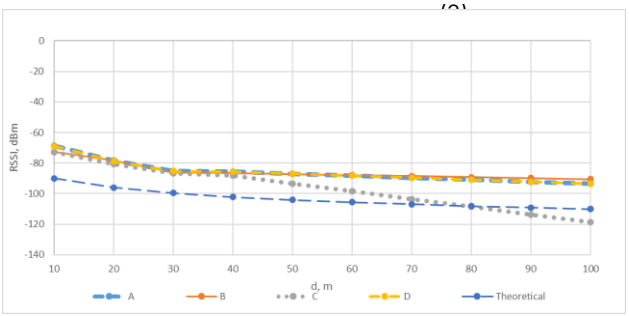

Figure 13 Comparison between measured and theoretical RSSI values at Locations A, B, C, and D plotted against distance

Figure 13 Comparison between measured and theoretical RSSI values at Locations A, B, C, and D plotted against distance shows the theoretical and measured RSSI for different distances and locations. It is found that the RSSI is inversely proportional to the distance between the module and the receiver. At a distance below 40 m, the RSSI at all locations are similar. However, when the distance increases above 40 m, the RSSI at Location C drops linearly to the distance compared to other locations. Location C shows a linear drop in the RSSI value because the

module is located near the traffic flow. The RSSI readings collected at the Locations A, B, and D are very close. It is found that the theoretical RSSI is lower than the measured RSSI, which is due to the antenna gain used in the actual measurement.

Based on the comparison between actual measurement and simulation, it is found the simulated bandwidth from COMSOL is 215.37 MHz, while the measured bandwidth is way off than otherwise provided by Nordic, which is 125 MHz. Besides that, the simulated resonance frequency of 2.407 GHz is about 3.53% away from the measured resonance frequency, 2.49 GHz from the portable Spectrum Analyzer. It could be due to the insufficient objects in the model, differences in ground plate dimensions, differences in via numbers, spacing and radius, and slight differences in materials used.

Besides that, the antenna model defined in the simulation only includes the FR-4 substrate, the MIFA antenna, the ground plates and the vias. The simulation does not include other components such as transceiver IC, capacitors, resistors, traces, plastic casings in which the module is encased within, and the coatings on the PCB, affecting the antenna performance [18][19]. When these components are included into the model in COMSOL, it increases the simulation time and computational cost, hence it is not considered in the simulation.

The shape of the ground plane has significant effects on the antenna's performance [20]. The authors of [21] had practically built multiple MIFAs with different ground plane sizes and found that all three antennas have different resonance frequencies. The larger the size of the ground plane the smaller the resonance frequency. It is advised to place as many vias as possible with spacing less than 1/20 of the operating wavelength [21]. This reduces parasitic impedance due to current loops that may further cause impedance mismatch. One study [22] had done some simulations on the signal integrity performance of PCB with slotted ground and had concluded that with the correct via spacing can reduce unwanted radiation, improves maximum distortion, jitter and noise margin characteristics.

FR4 substrate's dielectric constant (Dk) varies from manufacturer to manufacturer. Different manufacturers of the PCB may use different techniques to produce their FR4 differently [23], possibly to meet their clients' various requirements. The relative permittivity and other relevant physical constants that were given by COMSOL may not be the same as the one used by Nordic. Hence, the differences in the dielectric constant (Dk) may cause a slight difference in the simulated results.

Discussions of discrepancies aside, the 3D far-field gain of the simulation is matching well with the radiation pattern of a 1/4 λ monopole antenna. At the resonance frequency of 2.407 GHz, the 2D far-field gain are positive for both lobes, indicating that the antenna is radiating along the X-axis. The computed directivity at 2.402 GHz is $\theta = 4.0909^{\circ}$, $\varphi = 224^{\circ}$, and magnitude = 1.8964 dB. This result is consistent with the workings of the NRF24L01 module, where it can act as both transmitter and receiver.

4.0 CONCLUSION

This work has reported the radiation characteristic of a cloud-based magnetometer for vehicle detection. Unlike the other traffic monitoring system that utilizes CCTV and video image detectors, the proposed magnetometer detects the vehicle based on a magnetic sensor system, Arduino pro-mini and nRF24L01. The signal from the magnetic sensor is processed by the microcontroller and transmitted through nRF24L01 transceiver by a MIFA antenna. The taper design at the feeding of MIFA antenna enhances the return loss and affects its resonance frequency. The lowest return loss can be achieved when the taper length is 20 mils, and with that taper length, the operating bandwidth of the antenna increase to 215.37 MHz. The simulated 3D and 2D gain radiation patterns have validated the omnidirectional radiation characteristic of the MIFA antenna. Based on the simulation, it is found that the highest antenna gain is at its resonance frequency, which is 2.4 GHz. Based on the experimental measurement, it is found that in the range of 40 m, the measured RSSI is uniform surrounded antenna. However, as the distance increases continuously above 40 m, the RSSI near the traffic flow drops significantly compared to the other direction.

Acknowledgement

Communication of this research is made possible through monetary assistance by Universiti Tun Hussein Onn Malaysia and the UTHM Publisher's Office via Publication Fund E15216.

References

[1] C. Güven, Ö. Karaduman, and E. Avci. 2021. A Review on Urban Intelligent Traffic Management Problems: Sensors and Methods. *2021 2nd International Informatics and Software Engineering Conference (IISEC)*. 1-6. https://doi.org/10.1109/IISEC54230.2021.9672412.

[2] M. Grote, B. Waterson, and F. Rudolph. 2021. The Impact of Strategic Transport Policies on Future Urban Traffic Management Systems. Transp. Policy. 110: 402-414. https://doi.org/10.1016/j.tranpol.2021.06.017.

[3] M. Shahgholian and D. Gharavian. 2018. Advanced Traffic Management Systems: An Overview and a Development Strategy. arXiv Prepr. arXiv1810.02530.

[4] Honeywell. 2012. Three-Axis Digital Compass IC HMC5883L. HMC5883L Data Sheet. 1-19.

[5] Arduino. 2022. Arduino Pro Mini. 1-9. Arduino. Accessed: Jan. 10, 2022. [Online.] Available: https://docs.arduino.cc/retired/boards/arduino-pro-mini.

[6] Texas Instruments. 1997. High Speed CMOS Logic Analog Multiplexers/demultiplexers. 74HC4051 Datasheet, Nov. 1997 [Revised Sept. 2002].

[7] D. Orfeo *et al*. 2018. Mechano-magnetic Telemetry for Underground Water Infrastructure Monitoring. *Front. Built Environ.* 4(29): 1-14. Doi:10.3389/fbuil.2018.00029.https://doi.org/10.3389/fbuil.2018.00029.

[8] Espressif Systems. 2020. ESP8266EX Datasheet. *Espr. Syst*. 31. [Online]. Available: https://www.espressif.com/sites/default/files/documentation/esp32_datasheet_en.pdf.

[9] R. H. Arjadi, H. Candra, H. D. Prananto, and T. A. W. Wijanarko. 2018. RSSI Comparison of ESP8266 Modules. *Electrical Power, Electronics, Communications, Controls and Informatics Seminar (EECCIS), 2018*. 150-153.

[10] R. W. Pryor. 2021. *Multiphysics Modeling using COMSOL 5 and MATLAB.* 2nd Ed. Mercury Learning and Information.

[11] L. Wezranovski, Z. Urban, L. Ivanek, and Y. Zakaria. 2016. Patch Antenna Optimization in COMSOL Multiphysics. *ELEKTRO*. 104-109. https://doi.org/10.1109/ELEKTRO.2016.7512045.

[12] S. Sharma, C. C. Tripathi, and R. Rishi. 2017. Impedance Matching Techniques for Microstrip Patch Antenna. *Indian J. Sci. Technol.* 10(28): 1-16. https://doi.org/10.17485/ijst/2017/v10i28/97642.

[13] A. Massaccesi and P. Pirinoli. 2018. Enhancing the Bandwidth in Transmitarray Antennas using Tapered Transmission Line Matching Approach. *12th European Conference on Antennas and Propagation (EuCAP 2018)*. https://doi.org/10.1049/cp.2018.0426.

[14] D. F. Mamedes, J. P. F. da Silva, J. da Silva Souza, T. da Silva Evangelista, T. R. de Sousa, and P. H. da Fonseca Silva. 2017. Analysis of Impedance Matching Techniques in Tapered Microstrip Patch Antenna. *2017 SBMO/IEEE MTT-S International Microwave and Optoelectronics Conference (IMOC)*. 1-4. https://doi.org/10.1109/IMOC.2017.8121034.

[15] O. Losito, V. Dimiccoli, and D. Barletta. 2014. Meander-line Inverted F Antenna Designed using a Transmission Line Model. *The 8th European Conference on Antennas and Propagation (EuCAP 2014)*. 1370-1373. https://doi.org/10.1109/EuCAP.2014.6902033.

[16] D. M. Pozar. 2012. *Microwave Engineering*. Wiley.

[17] R&S FSH4/8/13/20. 2022. Spectrum Analyzer Operating Manual, Version 37. Rohde and Schwarz, Munich, Germany, 2022. Accessed: Feb. 25, 2022. [Online]. Available: https://scdn.rohde-schwarz.com/ur/pws/dl_downloads/dl_common_library/dl_manuals/gb_1/f/fsh_1/FSH_OperatingManual_en_FW3.40.pdf.

[18] T. Q. K. Nguyen, M. S. Miah, L. Lizzi, K. Haneda, and F. Ferrero. 2020. Experimental Evaluation of User's Finger Effects on a 5G Terminal Antenna Array at 26 GHz. *IEEE Antennas Wirel. Propag. Lett.* 19(6): 892-896. https://doi.org/10.1109/LAWP.2020.2973538.

[19] K. Wong and Y. Wu. 2016. Small-size Dual-wideband IFA Frame Antenna Closely Integrated with Metal Casing of the LTE Smartphone and having Decreased User's Hand Effects. *Microw. Opt. Technol. Lett.* 58(12): 2853-2858. https://doi.org/10.1002/mop.30165.

[20] N. A. Aboserwal, C. Balanis, and C. R. Birtcher. 2013. Impact of Finite Ground Plane Edge Diffractions on Radiation Patterns of Aperture Antennas. *Prog. Electromagn. Res. B.* 55: 1-21. https://doi.org/10.2528/PIERB13082702.

[21] G. T. Tapan Pattnayak. 2018. AN91445 Antenna Design and RF Layout Guidelines Authors: Tapan Pattnayak, Guhapriyan Thanikachalam Associated Part Family: CY8C4XXX-BL, CYBL1XXXX, CY8C6XXXXX-BL. Antenna Des. RF Layout Guidel. 001: 1-60.

[22] S. Lee, W. Seo, and J. Choi. 2010. The Effect of Via Spacing on the Signal Integrity Performance of PCB with Slotted Ground. *IEICE Proc. Ser.* 52(2WD1-1).

[23] M. Yogendrappa. 2022. Why FR4 Material is Commonly used in PCB Fabrication? Sierra Circuit. Accessed: March. 15, 2022. [Online.] Available: https://www.protoexpress.com/blog/why-fr4-material-in-pcb-fabrication/.